Applied Catalysis B: Environmental 179 (2015) 150–159

Contents lists available at ScienceDirect

Applied Catalysis B: Environmental

journal homepage: www.elsevier.com/locate/apcatb

Coprecipitation versus chemical vapour deposition to prepare Rh/Ni bimetallic catalysts

Patricia Benito[a,*], Vladimiro Dal Santo[b,**], Valentina De Grandi[c,1], Marcello Marelli[b], Giuseppe Fornasari[a], Rinaldo Psaro[b], Angelo Vaccari[a]

[a] Dipartimento di Chimica Industriale "Toso Montanari", Alma Mater Studiorum–Università di Bologna, Viale Risorgimento 4, 40136 Bologna, Italy
[b] CNR – Istituto di Scienze e Tecnologie Molecolari, Via C. Golgi, 19, 20133 Milano, Italy
[c] Dipartimento di Chimica, Università degli Studi di Milano, Via G. Venezia, 21, 20133 Milano, Italy

ARTICLE INFO

Article history:
Received 23 January 2015
Received in revised form 4 May 2015
Accepted 6 May 2015
Available online 7 May 2015

Keywords:
Hydrotalcite-type
Ni/Rh
Coprecipitation
Chemical vapour deposition
Catalytic partial oxidation of methane

ABSTRACT

The Rh/Ni interaction in bimetallic Rh/Ni/Mg/Al hydrotalcite-type (HT) derived catalysts for the catalytic partial oxidation (CPO) of CH_4 was studied modifying the preparation method. The conventional incorporation of both Rh and Ni by coprecipitation (CP) of HT precursors was compared with the addition of Rh by chemical vapour deposition (CVD) to reduced Ni/Mg/Al HT-derived catalysts. Two Ni loadings were selected (about 8 and 2 wt.%), whereas the Rh content was kept constant (0.18 wt.%). Ni- and Rh-monometallic catalysts were prepared as reference materials.

The addition of Rh resulted in an increase in Ni reducibility and dispersion for both CP and CVD catalysts. The Rh/Ni interaction was stronger in CP catalysts, while in CVD ones Rh overspread either on the support or Ni particles, with a preferential deposition on the latter. The Ni loading, regardless of the Rh incorporation method, was the main factor to determine the formation and growth of metallic particles. CO-DRIFTS spectra revealed that the dispersing and reducibility effect of Rh was more evident in the samples with a lower Ni-loading.

The small amount of Rh in the catalysts yielded to higher CH_4 conversions, especially in low Ni-containing catalysts wherein the Ni^0 oxidation was avoided. All the catalysts were activated during catalytic tests at high temperature by reduction of hardly reducible species. The strongest Rh/Ni interaction in CP catalysts yielded to better performances with a lower carbon formation and high resistance towards metallic particle sintering.

1. Introduction

Bimetallic noble metal/nickel catalysts were used in H_2 production catalytic processes [1,2] with the aim to improve the properties and catalytic activity of Ni-based catalysts, without largely rising the catalyst prize. The addition of small amounts of noble metals, mainly Rh, to the catalyst formulation increased the Ni^{2+} reducibility [3–9] and Ni^0 dispersion [10–12], retarded the sintering [9,13], avoided Ni^0 oxidation under steam or oxygen atmosphere [11,14,15], and decreased the activation energy for CH_4 dissociation in Rh/Ni alloys [16]. Consequently, enhanced activities were reported not only in conventional and commercial H_2 and syngas processes such as steam reforming [17,18], autothermal reforming [7,12,17,19,20] and oxyreforming [21–24], but also in more prone to carbon formation processes such as dry reforming [9,25–31], ethanol reforming [32–34], biogas reforming [35] and, lastly, in fuel cell devices [17], in which large hydrocarbons were fed in systems operating under transient conditions [36,37]. Indeed, Rh promoted the gasification of adsorbed carbon by steam in the autothermal reforming of isooctane [38] and decreased carbon formation in the reforming of liquid hydrocarbons [39]. Moreover, Rh improved sulphur tolerance during steam reforming of methane [40] or S-containing liquid fuels [41].

In particular, the synergetic effects between Rh and Ni were evidenced in the catalytic partial oxidation of CH_4, where Ni-based catalysts, although largely employed [42], suffered from deactivation by coke formation, sintering and oxidation [43]. The presence of both Rh and Ni increased the CPO activity in O_2-rich conditions, avoided the oxidation and led to a high stability towards coke formation [44–46]. Moreover, during temperature programmed surface reaction (TPSR) [47] and temperature programmed cat-

* Corresponding author. Tel.: +39 512093677; fax: +39 512093679.
** Corresponding author. Tel.: +39 250314428; fax: +39 250314405.
E-mail addresses: patricia.benito3@unibo.it (P. Benito), v.dalsanto@istm.cnr.it (V. Dal Santo).
[1] Currently at: Total Research & Technology Gonfreville, BP 27, 76700 Harfleur, France.

http://dx.doi.org/10.1016/j.apcatb.2015.05.016
0926-3373/

alytic partial oxidation, a drop in the light-off temperature was reported [48]. Lastly, the thermal profile along the catalyst bed and maximum temperature were modified [45,49]. Rh played a double role in bimetallic catalysts [50]: regardless of the concentration it promoted the reduction of the inactive $NiAl_xO_y$ to metallic Ni under partial oxidation conditions; and only by increasing its amount, it promoted the CPO activity.

To shed light on the noble metal-Ni interaction, several in-situ and ex-situ techniques were used. The formation of an alloy was confirmed by EXAFS and XANES [7,22,37]. However, it was also reported that the amount of Ni-containing species involved in the Rh/Ni alloy was very low in comparison to the total number of present species; whereas some works reported the formation of Rh/Ni or Ru/Ni clusters by migration of metallic particles [10,25]. The alloy formation was also evidenced by vis-UV/ DR, XPS [50], TEM-EDS [28,51]. On the contrary, Dias and Assaf [12] did not observe any change in the CO adsorption on Ni by CO-DRIFTS spectra, indicating that the noble metal (Pt, Pd or Ir) at low loadings did not modify significantly the electronic properties of Ni. Likewise, in some works [9,52,53], an interaction between Rh and Ni was stated, although without any conclusive evidence of Rh/Ni alloy formation in the catalysts.

The bimetallic noble metal/nickel catalysts preparation was mainly performed by sequential [12,20] or simultaneous impregnation [9,17,42,54], although bulk catalysts also showed good performances. Rh^{3+} and Ni^{2+} cations were simultaneously introduced in the hydroxyl layers of hydrotalcite-type (HT) compounds during coprecipitation [7,19,44,55]. After calcination and reduction, well stabilized metallic particles in an oxide matrix (MgO- and/or $MgAl_2O_4$-type phases) were obtained. On the other hand, the noble metal can be added to a calcined Ni-HT [36,37,46,56]. Moreover, Rh/Ni ceria-zirconia bulk catalysts were prepared by a pseudo sol-gel method [51,57,58] or by firstly introducing Ni during the sol-gel preparation and after impregnating Rh ions [26,30].

Hence, the contradictory characterization results may be related to the synthesis procedure; more specifically, the type of impregnation [5,19,22,24,59], the precursors [10], and the support [23,53,60]. Moreover, the noble metal/nickel ratio [54,61], the kind of noble metal [5,10,12] and the activation step (reduction) [42] may determine the interaction between the metals.

The aim of this work was to study the Rh/Ni interaction adopting a different approach. Bimetallic catalysts were prepared by: (1) conventional coprecipitation (CP), wherein both Rh and Ni were inserted in HT precursors and catalysts were obtained by calcination at high temperature; (2) chemical vapour deposition (CVD) of Rh-containing species over reduced Ni-based catalysts obtained from HT precursors as well. The HT precursors were intercalated with silicates rather than carbonates to improve the mechanical properties of the catalysts [62,63]. The deposition of Rh performed by CVD [64–66] was aimed to evaluate if Rh may be deposited on previously segregated Ni^0 particles [67,68] and it was able to modify the metal particle size and dispersion. By this way, the role of Rh (0.18 wt.%) on the reducibility, metal particle dispersion and performances of catalysts with different Ni loadings (about 8 and 2 wt.%) was investigated. For comparison purposes, monometallic Rh- and Ni-based catalysts were also studied.

2. Experimental

2.1. Synthesis

2.1.1. Coprecipitated catalysts

Ni/Mg/Al and Rh/Ni/Mg/Al HT precursors intercalated with silicate anions were synthesized by coprecipitation at constant pH [62]. The Ni/Mg/Al atomic ratio % (a.r.%) of the HT precursors were 8/60/32 and 2/66/32, whereas for the Rh/Ni/Mg/Al bimetallic precursors the a.r.% were 0.1/8/60/31.9 and 0.1/2/66/31.9. In the Rh/Mg/Al HT the a.r.% was 0.1/68/31.9. A 2 M solution containing the nitrates of the cations [$Mg(NO_3)_2{\cdot}6H_2O$, $Al(NO_3)_3{\cdot}9H_2O$, $Ni(NO_3)_2{\cdot}6H_2O$, $Rh(NO_3)_3$ (10 wt.% Rh in HNO_3)] in the appropriate ratios was slowly added to a 1 M solution containing silicates [sodium silicate solution, NaOH (≥10 wt.%), SiO_2 (≥27 wt.%)]. The pH was kept constant (10.5 ± 0.2) by NaOH dropwise addition. The obtained precipitate was kept in suspension under stirring at 60 °C for 45 min, then filtered and washed with distilled water until a Na_2O content lower than 0.02 wt.% was obtained. The precipitate was dried overnight at 60 °C. Catalysts were obtained by calcination (heating rate 10 °C/min) from room temperature to 900 °C and kept at this temperature for 12 h. The catalysts were named as follow: Ni8-CP, Ni2-CP, Rh-CP, RhNi8-CP and RhNi2-CP.

2.1.2. CVD catalysts

Ni-based catalysts, Ni8-CP and Ni2-CP, obtained by coprecipitation were previously reduced in H_2 flow (50 mL/min) at 750 °C for 12 h (heating rate 3 °C/min) and then cooled in H_2 flow in a tubular quartz reactor. Rh (0.18 wt.%) was deposited by CVD of $Rh(acac)(CO)_2$ and then reduced in H_2 at 500 °C for 1 h (heating rate 2.5 °C/min) [64,65]. Samples were recovered in a dry-box under Ar atmosphere and named as follows: RhNi8-CVD and RhNi2-CVD. A monometallic Rh-CVD sample (Rh 0.18 wt.%) was prepared by CVD of $Rh(acac)(CO)_2$ on a HT precursor Mg/Al = 68/32 a.r.% calcined at 900 °C.

2.2. Characterization techniques

Powder X-ray diffraction (PXRD) analyses were carried out using a Philips PW1050/81 diffractometer equipped with a graphite monochromator in the diffracted beam and controlled by a PW1710 unit (λ = 0.15418 nm). A 2θ range from 10° to 80° was investigated at a scanning speed of 70 °/h. Specific surface area (S_{BET}) measurements were carried out using a Micromeritics ASAP 2020 instrument. Samples were previously degassed under vacuum, heated up to 250 °C and maintained for 30 min. Chemisorption measurements of H_2 were carried out by a Micromeritics ASAP 2020 instrument using a conventional static method. The samples were reduced for 2 h at 750 °C in pure H_2 and cooled to room temperature (r.t.) under vacuum. The H_2 adsorption isotherm was established at 35 °C. After evacuation at r.t. a second H_2 isotherm was collected. By taking the differences between the two isotherms, the amount of irreversibly adsorbed H_2 was determined. The gas uptake by the metallic phase was obtained by extrapolating to zero pressure. The metal surface area and dispersion were determined from the H_2 chemisorption data, using a 1/1H/Metal (Rh + Ni) titration stoichiometry [25,69]. Metallic surface area per gram of metal was calculated considering that the metals were evenly distributed and nominal metal loading. DRIFTS analyses were performed in a home-made DRIFTS cell under inert gas where 20–40 mg of samples were loaded. Before performing CO-pulses experiments, the catalysts (pre reduced ex situ as reported in Section 2.1.2) were in situ reduced at 500 °C for 1 h under a 20 mL/min H_2 flow, with a heating rate of 10 °C/min and then cooled in a He flow (20 mL/min). DRIFT spectra were recorded after each pulse (CO/Ar = 49.8/50.2 v/v %); the gas streaming was monitored by means of a quadrupole mass spectrometer (HPR-20 QIC gas analysis mass spectrometer system/hiden analytical). The whole apparatus was previously described elsewhere [70,71]. Ni^0/Ni^{n+} ratios ($0 < n < 2$) were calculated as the ratio between integrated area of DRIFT bands of linear CO adsorbed on Ni^0 and those of CO adsorbed on highly or (highly + moderately) dispersed Ni^{n+} species. Integrated area of IR bands were obtained by peak fitting of DRIFT spectra using GRAMS™ software package.

Table 1
Specific surface area (S_{BET}) before (fresh) and after the catalytic tests (spent) and H_2 and CO chemisorption results on freshly reduced catalysts (before catalytic tests).

	N_2 adsorption/desoprtion		H_2 chemisorption		CO chemisorption	
Sample	S_{BET} fresh/m^2g^{-1}	S_{BET} spent/m^2g^{-1}	Metal dispersion/%	Metallic surface area/$m^2g^{-1}{}_{metal}$	$mmol_{CO}/g_{sample}$	$mmol_{CO}/mol_{Ni}$[a]
Ni2-CP	112	91	3.6	24	0.004	0.013
RhNi2-CP	122	114	4.4	29	0.016	0.048
RhNi2-CVD	130	112	4.7	31	0.015	0.044
Ni8-CP	96	95	5.1	39	0.019	0.014
RhNi8-CP	105	105	6.0	40	0.030	0.021
RhNi8-CVD	100	81	5.8	39	0.026	0.019
Rh-CP	100	101	9.2	41	–	–

[a] $mmolCO/mol_{Ni}$ ratios for bimetallic Rh/Ni samples calculated without considering Rh contribution.

Morphology and distribution of supported metal particles were evaluated by transmission electron microscope (TEM) micrographs. TEM micrographs of Ni8-CP (calcined, reduced and spent), RhNi8-CVD (spent) and RhNi2-CVD (reduced and spent) were taken in a ZEISS LEO120 TEM. The finely powder samples of RhNi8-CP (reduced and spent) and RhNi8-CVD catalyst after reduction were instead analyzed by a ZEISS LIBRA200FE TEM. A drop of the suspension was deposited on the carbon grid which, after solvent evaporation under vacuum, was inserted in the TEM column. In order to have a direct morphological comparison, all the pictures were taken at 25,000–50,000× magnifications, under the same optical conditions, spanning wide regions of several support grains to provide a well representative map of the catalysts. Electron Spectroscopic Imaging (ESI) collected with the in-column energy filter of ZEISS LIBRA200FE gave the elemental maps for Ni and Rh.

Size distribution histograms of metal particle diameters, evaluated from about 300–550 counts per sample, exhibited peaks centred on the reported median values (Fig. S3 and Table S3). We chose to use the median value instead of the calculated mean value to compare the size values, because the distributions were not always symmetric.

2.3. Catalytic tests

Catalytic partial oxidation (CPO) tests of CH_4 were carried out in a quartz reactor (i.d. 8 mm) filled with 0.5 g of catalyst (bed length 2 cm ca.), with particle size between 0.60 and 0.42 mm to avoid any pressure drop. The reactor was inserted in an electric oven. The maximum gas phase temperature (T_{max}) and the gas phase temperature at the outlet of the catalytic bed (T_{out}) were measured by a moveable chromel–alumel thermocouple, sliding in a quartz wire inside the catalytic bed. Catalysts were activated in situ by reduction with a H_2/N_2 = 50/50 v/v % gas mixture (7 L/h) at 750 °C for 12 h. Catalytic tests were performed at two oven temperatures, 500 and 750 °C, whereas the temperature inside the catalytic bed varied depending on the exo- or endothermicity of the reactions taking place. The catalyst was heated in a He flow up to reach the set temperature and then CH_4 and O_2 were fed. Catalytic tests were carried out by modifying the CH_4/O_2/He gas mixture (CH_4/O_2/He = 2/1/40, 2/1/20, 2/1/4 and 2/1/1 v/v) and the contact time value (τ, calculated as weight of catalyst on total flow at r.t.). Tests at low oven temperature (500 °C) were performed by feeding diluted gas mixtures [CH_4/O_2/He = 2/1/40 v/v (τ = 35 and 17 ms) and 2/1/20 v/v (τ = 65 and 35 ms)] to highlight the differences among catalysts. On the other hand, tests at high oven temperature (750 °C) with concentrated mixtures [CH_4/O_2/He = 2/1/4 v/v (τ = 65 ms) and 2/1/1 v/v (τ = 50 ms)] allowed to study the stability of the catalysts. Reaction products were analyzed on-line after water condensation by two gas chromatographs equipped with HWD and carbosieve SII columns, using He as carrier gas for the analysis of CH_4, O_2, CO and CO_2 and N_2 as carrier gas for the H_2 analysis. In all the catalytic tests the O_2 conversion was complete and the C balance between 98 and 102%.

3. Results and discussion

3.1. Characterization of catalysts

PXRD patterns (Supplementary Fig. S1) did not show any differences among Ni- and RhNi-based catalysts obtained by CP due to the low Rh content (0.18 wt.%). Diffraction lines due to forsterite (Mg_2SiO_4), rock-salt and defective spinel phases were identified, characteristic of solids obtained by high temperature calcination of silicate-intercalated HT precursors [62]. Otherwise, in PXRD patterns of CVD bimetallic Rh/Ni catalysts lines ascribed to Ni^0 were observed, since these samples were prepared by CVD of Rh^{3+}-containing species over reduced monometallic Ni8-CP and Ni2-CP catalysts. All the catalysts showed high specific surface area values (ca. 100 $m^2\,g^{-1}$) considering the calcination temperature (900 °C), without any surface area decrease during the CVD process (Table 1).

Temperature reduction profiles of monometallic and bimetallic coprecipitated catalysts were displayed in Fig. 1. The onset and maximum of H_2 consumption peaks, attributed to the reduction of Ni species in the spinel or rock-salt structure [63], shifted towards lower temperatures by Rh inclusion. This feature was more remarkable for the RhNi2-CP catalyst because of the higher Rh/Ni molar ratio. The enhanced Ni reduction by Rh suggested a close interaction between both elements to allow the H_2 spillover from noble metal to nickel on the catalyst surface.

Metal dispersion and metallic surface area values of CP and CVD samples were summarized in Table 1. It is worth noting that in HT-derived bulk catalysts, these values may depend not only on the metal particle size but also on the reducibility degree of Ni species

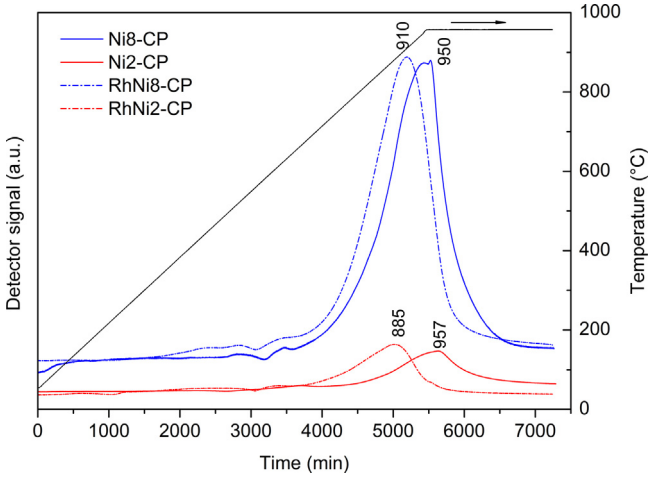

Fig. 1. H_2 temperature programmed reduction (TPR) profiles of coprecipitated mono- and bimetallic catalysts.

Table 2
Assignment of the IR bands (cm^{-1}) to the related species in the different catalysts.

Species	Ni2-CP	RhNi2-CP	RhNi2-CVD	Ni8-CP	RhNi8-CP	RhNi8-CVD	RhNi2CVD[a]	RhNi8CVD[a]
Ni^0 (Ni_3CO, Ni_4CO)	1886	1860	1863	1837	1840-1863	1843-1887	1852	1864
$Ni_2{}^0CO$	1910	1903	1903	1902	1900	1908	1905	1909
$Ni_2{}^{\delta+}CO$	1942	1957	1957	1935	1951	1952	1942	1949
Ni^0-CO		2027	2034	2030		2033	2030	2031
$Ni^{\delta+}$-CO	2040				2044			2044
$Ni^{\delta+}$-CO moderately dispersed		2062	2063	2049		2069	2058	2067
$Ni^{\delta+}(CO)_3$, $Ni^{\delta+}(CO)_2$	2077			2068	2078	2069		
$Ni^{\delta+}(CO)_3$, $Ni^{\delta+}(CO)_2$ highly dispersed	2090	2093	2089		2089	2093		

[a] After catalytic tests.

and the accessibility of the H_2 to them. In particular, in the catalysts here investigated, the presence of hardly reducible Ni species into spinel- or MgO-type phases [63] may be responsible of the small dispersion values reported in Table 1, rather than the presence of large metallic particles; although the inaccessibility of some metallic particles due to the embedment in the support cannot be ruled out. These factors may also explain the lower dispersion and metallic surface values of low-loaded than high-loaded Ni catalysts. On the other hand, the increase in dispersion due to the presence of Rh, more remarkable for RhNi2-CP and RhNi2-CVD catalyst, may be related to an increase of the metal fraction in the catalysts or to the formation of smaller Ni^0 particles. Moreover, if bimetallic nanoparticles were obtained during reduction at 750 °C, a Ni surface enrichment, due to the lower sublimation enthalpy of Ni than that of Rh [69], may not be excluded, altering H_2 chemisorption results.

IR spectra of adsorbed CO are very sensitive to changes in electronic density (i.e., charge), size and morphology of supported metal nanoparticles. The ratio between linear and bridged CO may be related to particle size (i.e. the lower the particle size, the higher the ratio); increase in electronic density usually results in a shift to lower wavenumbers of linear CO bands, while its decrease has the opposite effect on band shift. Hence, to shed light on the catalyst properties CO-DRIFTS and TEM analyses were performed on reduced samples.

CO-DRIFTS spectra of Ni-containing catalysts were displayed in Fig. 2. The assignment of the bands, made on the basis of available literature and from the spectral fitting results, was summarized in Table 2. The high-loaded Ni8-CP monometallic catalyst spectrum showed a narrow band at 2030 cm^{-1} attributable to linearly adsorbed CO on low dispersed Ni^0 (Fig. 2A). On the contrary, 2068 and 2049 cm^{-1} (sh) signals, related to more dispersed particles, were sensibly less intense. More in detail, the band at 2068 cm^{-1} may be attributed to highly dispersed polycarbonyl species of partially positive Ni, as $Ni^{\delta+}(CO)_3$, $Ni^{\delta+}(CO)_2$ [72]. Species adsorbed on Ni^0 particles also emerged from bridged-CO zone at 1935, 1902 and 1837 cm^{-1}, representative of multi-centred species, such as Ni_3CO and Ni_4CO [73], or of bridged-CO, adsorbed on different crystalline facets [12]. Hence, the Ni8-CP catalyst was mainly constituted of both large Ni^0 nanoparticles and highly dispersed partially oxidized Ni particles.

The spectra of Ni2-CP sample (Fig. 2B) showed an increase of the bands ascribable to CO adsorbed on highly dispersed partially positive Ni [72], located at 2200, 2090 and 2077 cm^{-1}, with respect to the band at 2040 cm^{-1} ascribable to linear-CO species chemisorbed on moderately dispersed $Ni^{\delta+}$ sites [12,73]. Very intense bands were present also in the bridged-CO region, with the components at 1942, 1910 and 1886 cm^{-1}. The high frequency bands were more intense than the low frequency ones if compared with those of Ni8-CP sample. These data accounted for the presence of dispersed Ni-containing particles, with a low fraction of fully reduced Ni^0 species, in low loaded samples.

By comparing the Ni8-CP and Ni2-CP samples, CO-DRIFT data confirmed that increasing the metal loading, Ni-containing species gained a higher metallic character and/or less dispersed fraction, since all the bands moved towards lower wavenumbers. However, the lack of a significant change of bridged/linear CO area ratio (Table 3) strongly suggested that the differences in metallic dispersion between Ni2-CP and Ni8-CP samples, may be related to differences in the reducibility degree rather than to different metallic particle size.

When bimetallic Rh/Ni samples were considered, some differences arose depending on both Rh deposition method and Ni loading (Fig. 3). In RhNi8-CP sample (Fig. 3A) two convoluted main bands were observed in linear CO region, closely resem-

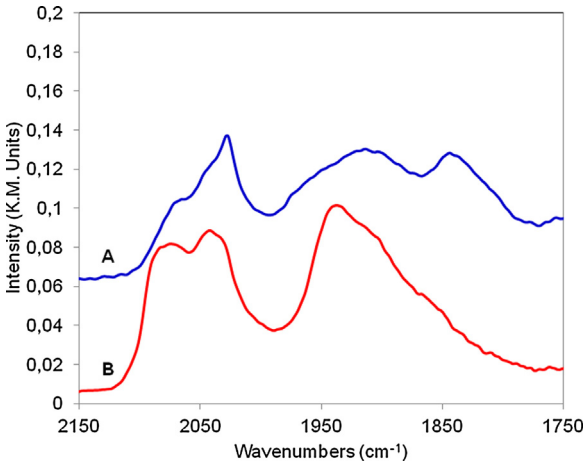

Fig. 2. CO-DRIFT spectra of Ni8-CP (trace A, blue line) and Ni2-CP (trace B, red line) reduced catalysts. (For interpretation of the references to colour in this figure legend, the reader is referred to the web version of this article.)

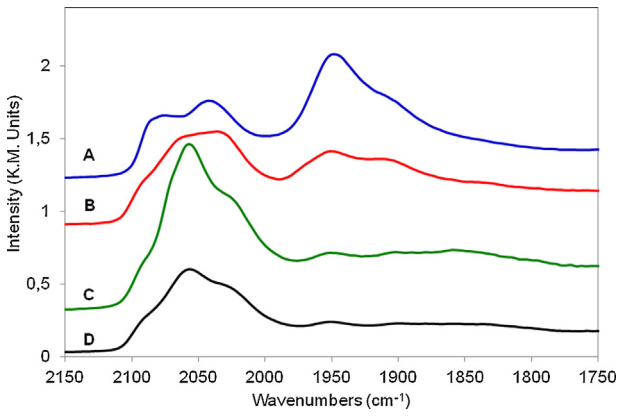

Fig. 3. CO-DRIFT spectra of RhNi8-CP (trace A, blue line), RhNi8-CVD (trace B, red line); RhNi2-CP (trace C, green line) and RhNi2-CVD (trace D, black line) reduced catalysts. (For interpretation of the references to colour in this figure legend, the reader is referred to the web version of this article.)

Table 3
Integrated areas and ratio values related to linear and bridged CO species (B/L) and to linear CO adsorbed on zerovalent ($L_{Ni(0)}$) and highly dispersed / total (highly and moderately dispersed) oxidized ($L_{Ni(n+)}$) Ni sites.

Sample	Linear CO	Bridged CO	B/L ratio	$L_{Ni(0)}/L_{Ni(n+)}$ highly dispersed/total
Ni2-CP	1.38	2.44	1.77	3.6/0.7
RhNi2-CP	20.85	0.64	0.031	9.5/0.8
RhNi2-CVD	10.51	0.26	0.025	7.3/2.3
RhNi2-CVD spent	4.32	~0.00	~0.00	[a]/0.9
Ni8-CP	0.65	1.13	1.74	[a]/1.3
RhNi8-CP	6.44	22.08	3.43	13.4/1.7
RhNi8-CVD	10.15	7.64	0.75	10.6/1.4
RhNi8-CVD spent	3.49	2.42	0.69	[a]/3.7
Rh CVD	0.55	–[c]	–	0.2[b]
Rh CP	4.5	3.0	1.5	1.2[b]

[a] Highly dispersed $Ni^{\delta+}$ sites not revealed.
[b] Rh(0)/Rh(I) ratio.
[c] Bridged CO not revealed.

bling those of Ni-based siliceous materials [72]. For these bimetallic systems the relative intensities of component bands at 2044 and 2078 cm^{-1} strongly depended on the reduction degree and particle dimensions, especially the latter band was predominant when Ni sites were only partially reduced (i.e. mostly $Ni^{\delta+}$), while the 2044 cm^{-1} signal seemed to be diagnostic of linear CO on $Ni^{\delta+}$ particles. Spectral fitting revealed also the presence of a minor band at 2089 cm^{-1} ascribable to $Ni^{\delta+}(CO)_3$ and $Ni^{\delta+}(CO)_2$ highly dispersed species. Regarding bridged CO species, the main band appeared at 1951 cm^{-1} attributable to a $Ni^{\delta+}$ fraction, while only a shoulder (1900 cm^{-1}) evidenced the presence of multi-centred carbonyls on Ni^0. Thus, the presence of Rh led to the formation of more dispersed Ni particles, although with a fraction of large $Ni^{\delta+}$ particles. It appeared that the more significant effect of Rh was exerted on the smaller particles rather than on larger ones.

RhNi8-CVD spectrum (Fig. 3B) was characterized by the presence of linear CO species chemisorbed on Ni^0 sites (pronounced 2033 cm^{-1} band) together with low fractions of moderately dispersed $Ni^{\delta+}$ sites (2069 and 2093 cm^{-1}) [72]. The coalescence of 2073 and 2039 cm^{-1} bands towards the 2069 cm^{-1} one was observed, suggesting that the electronic state of Ni moved towards slightly positive charge, although the formation of physisorbed $Ni(CO)_4$ cannot be excluded since its infrared signal falls at about 2060 cm^{-1} [28,74]. RhNi8-CVD sample presented a bridged CO zone analogous to that observed for the RhNi8-CP sample, but with a more intense band located at 1908 cm^{-1}, showing a larger component of reduced particles.

On the other hand, deep changes in CO-DRIFT spectra were provoked by the Rh incorporation in low Ni-loaded CP and CVD samples (Figs 3C and 3D), showing similar trends regardless of the preparation method, i.e. almost overlapped spectra resulted. The spectra of RhNi samples, both CP (Fig. 3C) and CVD (Fig. 3D), showed an intense band at ca. 2060 cm^{-1} with two shoulders at 2090 and 2027 cm^{-1}, due to CO adsorbed on partially reduced and zerovalent Ni sites. Spectral fitting revealed that the 2060 cm^{-1} band intensity was lower in CVD sample with respect to CP one. In the bimetallic samples the intensity of multi-centred carbonyls bands strongly decreased (bridged/linear CO ratios fell down from 1.77 to 0.30, such as reported in Table 3), only $Ni_2{}^{\delta+}$-CO band at 1957 cm^{-1} was still significant (Table 2). These data suggested that the Rh incorporation promoted a higher amount and better dispersion of Ni^0 particles, most efficiently for CP sample.

$Ni^0/Ni^{\delta+}$ ratios, calculated as detailed in Section 2 and reported in Table 3, suggested a more subtle effect of Rh addition, strongly depending on both preparation method (i.e. CP or CVD) and Ni loading. Parent monometallic Ni8-CP sample showed a lower amount of highly dispersed $Ni^{\delta+}$ if compared to Ni2-CP one. The addition of Rh by CP was more efficient in reducing the amount of highly dispersed $Ni^{\delta+}$ species, while the addition by CVD exerted its effect

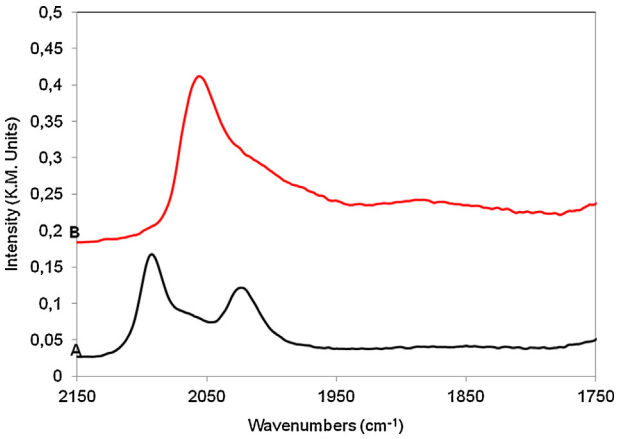

Fig. 4. CO-DRIFT spectra of Rh-CVD (trace A, black line) and Rh-CP (trace B, red line) reduced catalysts. (For interpretation of the references to colour in this figure legend, the reader is referred to the web version of this article.)

mostly on moderately dispersed $Ni^{\delta+}$ species (according to the preferential deposition of Rh on preformed metallic Ni NPs showed by TEM, see below). Finally, the effects due to Rh addition were, as expected and in agreement with TPR analysis, more evident on Ni2 sample in comparison to Ni8 one.

On-line QMS CO-pulses quantitative data (Table 1) confirmed a low CO adsorption, proportional to Ni-loading, by monometallic samples, the CO/Ni ratios resulting similar for both systems. The different methods of Rh addition gave rise to similar values of adsorbed CO-per-mole of Ni; RhNi2 catalysts showed a significant increase with respect to the RhNi8 ones.

For comparison purposes two monometallic Rh-containing catalysts, prepared by both CVD and CP methods, were analyzed by CO-DRIFTS (Fig. 4). The spectrum of Rh-CVD sample (Fig. 4A) showed the presence of an intense doublet located at 2090 and 2020 cm^{-1}, typical of $Rh(CO)_2$ species. The band located at 2060 cm^{-1}, attributable to linear CO adsorbed on Rh^0 sites, showed lower intensity [64]. On the contrary, the spectrum of Rh-CP (Fig. 4B) only showed an intense band located at 2060 cm^{-1} already attributed to CO on Rh^0 nanoparticles. Notably bands attributable to bridged CO on Rh^0 sites, falling around 1850 cm^{-1}, were not observed in reported spectra, evidencing the presence of only small Rh^0 nanoparticles, in agreement with the very low loading.

It is noteworthy that the presence of bands attributable to either Rh(I) isolated sites or Rh(0) sites of metallic NPs was never detected in the spectra of Ni/Rh bimetallic catalysts, probably due to the low Rh loadings and to the Rh/Ni mixing that resulted in very low intensity of such bands. For these reasons, in the discussion

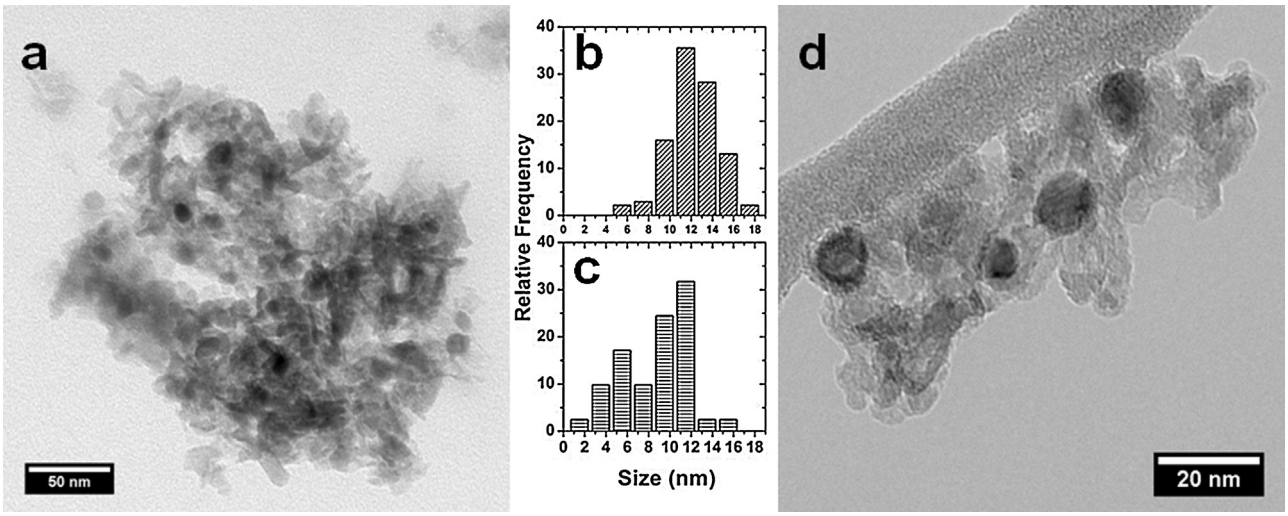

Fig. 5. HRTEM images and particle size distributions of Ni8-CP (a, b) and RhNi8-CP (c, d) reduced catalyst.

about CO-DRIFT spectra and CO-chemisorption only the data of Ni adsorption sites were taken into account.

The increase in dispersion due to the addition of small amounts of Rh and/or other noble metals to Ni-based catalysts was already reported in the literature [21]; the formation of a Rh/Ni alloy was invoked, in which Rh surface segregation inhibited the Ni particle growth and promoted their reduction because of electronic effect. Actually, Rh/Ni alloys show a miscibility gap (i.e. segregation can occur) at temperatures lower than 827 °C [75]. In this work, it was observed that the effect of Ni loading was determining for particle formation and growth. The dispersing effect of Rh resulted less evident in high-loaded samples, for which the largest effect was observed for smaller particles, although Ni redispersion in CVD samples was noticed.

To shed light on the effect of Rh on Ni particle size, TEM images of high loaded mono- and bimetallic catalysts were taken. TEM images for the Ni8-CP catalyst after reduction at 750 °C were shown in Fig. 5a. The metal particles were located both at the external surface of the oxide grains and embedded in their inside. Ni particles with an average size of 12.1 nm were observed (Fig. 5b), exhibiting well-formed fcc crystal habits with polyhedral sections. A Ni8-CP sample just after calcination at 900 °C was also measured as reference structure before the Ni^0 phase formation. A characteristic crystal powder diffraction pattern superimposed to an amorphous background was detected in electron diffraction mode, which was in agreement with the phases previously discussed for the calcined HT precursors. The support exhibited a mixture of small prismatic oxide crystalline grains (size 20–30 nm), aggregated in large and not homogeneous ensembles, and amorphous irregular size and shape areas. The smallest structures detected in the reduced sample images, whose attribution was not clear, were present also in the just calcined sample, so excluding their correspondence to very small Ni particles.

On the reduced RhNi8-CP bimetallic catalyst (Fig. 5d), the metal particle size distribution was very broad spanning from 2.4 nm to 14.5 nm, with an average diameter of 8.9 nm (Fig. 5c). The presence of small metal particles was well detected in the thin and amorphous region of the support.

On RhNi8-CVD after Rh deposition and reduction at 500 °C (Fig. 6), the metal particle average size was 12.2 nm, very close to that obtained in the Ni8-CP catalyst. ESI maps (Fig. 6c–e) highlights the uneven distribution of Rh that overspread on the support and Ni particles. However, a fine analysis of the ESI map revealed that a preferential deposition of Rh on Ni particles seemed to occur, since a higher Rh signal was detected in correspondence of Ni NPs (marked by the arrows in Fig. 6c and d).

In summary, from CO-DRIFTs and TEM characterization it appeared that the effect of Rh addition by CVD on prereduced Ni-containing catalysts mainly resulted in an increase of the amount of reduced Ni sites. When Rh and Ni ions were randomly distributed in the brucite-type layers of the HT precursors, this effect was more pronounced, the CP samples showing a higher fraction of reduced Ni and a higher dispersion. It is worth noting that for both CP and CVD catalysts, Rh/Ni ratio was the key factor to modify the Ni particle features.

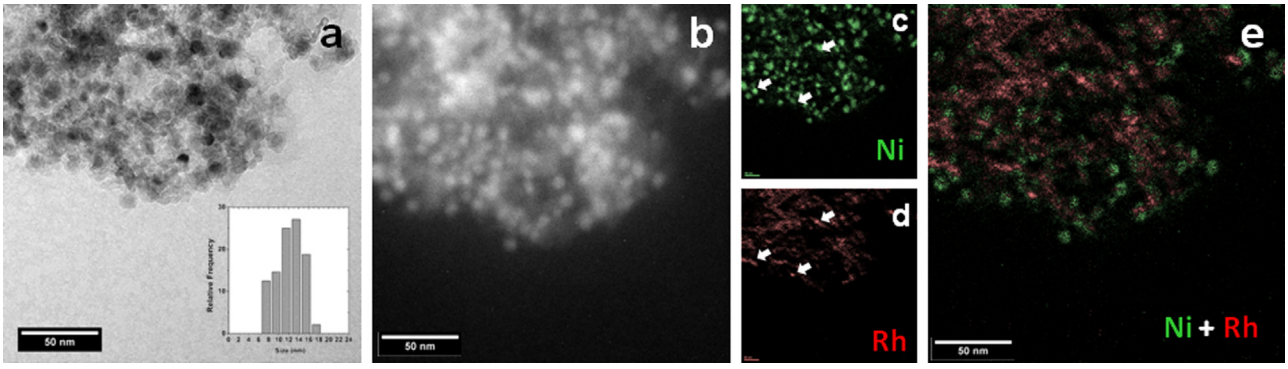

Fig. 6. HRTEM image (a), HAADF image (b) and ESI maps (c–e) of RhNi8-CVD reduced catalyst.

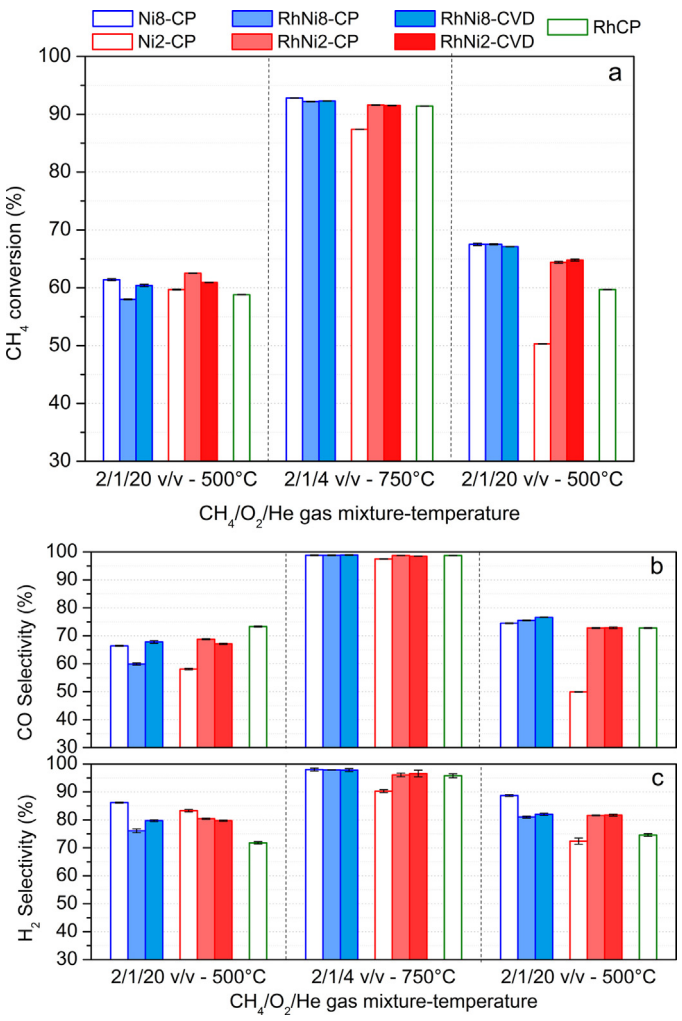

Fig. 7. CH_4 conversion (a) and selectivity in CO (b) and H_2 (c) obtained with Ni, Rh/Ni and Rh catalysts during tests at 65 ms contact time and modifying the T_{oven} (500 and 750 °C) and the CH_4/O_2/He gas mixture (2/1/20 and 2/1/4 v/v).

3.2. Catalytic partial oxidation tests

CPO tests were performed, as previously reported for monometallic Ni catalysts [63], to study the role of the preparation procedure on catalytic performances. The oven temperature was kept constant at 500 and 750 °C, while the gas mixture concentration (CH_4/O_2/He v/v) and the contact time value were modified. In Fig. 7 were displayed CH_4 conversions and syngas (CO and H_2) selectivities obtained at selected reaction conditions, namely during tests at 65 ms. H_2/CO ratio values and gas phase maximum temperatures for the reaction conditions displayed in Fig. 7, were summarized in Table 4.

Under the initial reaction conditions, CH_4/O_2/He = 2/1/20 v/v and T_{oven} = 500 °C, the gas phase temperatures in the first part of the catalytic bed were around 600–580 °C (Table 4) due to the exothermic reactions, while the temperatures recorded at the outlet were around 540–515 °C (Table S1). The addition of Rh increased the maximum gas phase temperature. Surprisingly, the bimetallic RhNi8-CP and RhNi8-CVD catalysts showed slightly lower CH_4 conversion values than the monometallic Ni8-CP catalyst. On the contrary, the presence of Rh into the low loaded RhNi2-CP sample increased the CH_4 conversion. The syngas produced was richer in H_2 than in CO, due to the contribution of the water gas shift (WGS) reaction. H_2/CO ratios were in the 2.33–2.60 range. The highest H_2 selectivity for monometallic Ni samples suggested that the inclusion of Rh decreased the contribution of the WGS and, therefore, the H_2/CO ratio. The coprecipitation led to better performances for low Ni loading, whereas the opposite trend was observed for high Ni-loaded catalysts.

Smaller, more dispersed and reduced Ni^0 particles in RhNi2-CP and RhNi2-CVD samples than in high-loaded ones, together with the presence of Rh, which increased the activity in comparison to Ni2-CP catalyst, may explain the improved performances of bimetallic low-loaded Rh/Ni catalysts. The small differences in catalytic performances between RhNi2-CP and RhNi2-CVD samples may be related to metal-support interaction, since CO-DRIFTS indicated that both samples had similar behaviours. On the other hand, for high loaded catalysts the different reduction, observed in CO-DRFITS, may explain their catalytic behaviour.

In tests at T_{oven} = 750 °C and with concentrated gas mixtures (CH_4/O_2/He = 2/1/4 and 2/1/1 v/v), the role of Rh was still evident; although the higher temperatures in the catalytic bed (Table 4 and S1) led to an increase in the performances and made it more difficult to discriminate among catalysts. The main differences between mono- and bimetallic catalysts were found for low Ni-loaded samples, Rh improved the activity and decreased the maximum temperature from 863 °C for Ni2-CP to ca. 829 °C for RhNi2-CP and RhNi2-CVD (Table 4). The product distribution roughly followed the same trend than conversion; however, the temperature determined the H_2/CO ratio, namely the production of CO increased due to reverse water gas shift (RWGS) reaction and the syngas had a H_2/CO of ca. 1.95.

When setting the initial reaction conditions after tests at high temperature, unlike Ni2-CP catalyst, no deactivation was observed for bimetallic catalysts. Indeed the colour change of Ni2-CP (but not of Ni8-CP) catalyst particles placed at the inlet of the bed, due to the oxidation of Ni^0 to Ni^{2+}, was not observed [63]. The higher amount of reduced nickel species in RhNi2-CP and RhNi2-CVD than in Ni2-CP, as well as the intrinsic activity in CH_4 conversion provided by Rh species [44], may have helped to stabilize reduced nickel species. Actually, RhNi2-CP and RhNi2-CVD samples, likewise Ni8 catalysts, activated with time-on-stream (TOS), a behaviour related to the reduction of the remaining hardly reducible Ni species under reaction conditions.

Lastly, it is worth noting that a monometallic Rh-CP catalyst at low temperature performed worse than mono- and bimetallic ones and gave rise to lower H_2 selectivity, but it was rather stable with TOS. Therefore, although the presence of the noble metal enhanced the performances, nickel species contributed significantly to the catalytic activity.

Table 4
H_2/CO ratios and gas phase maximum temperatures (T_{max}, °C) obtained with mono- and bimetallic catalysts during tests at 500 and 750 °C and 65 ms contact time, feeding different CH_4/O_2/He gas mixtures.

T_{oven}/°C	CH_4/O_2/He v/v	Ni8-CP		RhNi8-CP		RhNi8-CVD		Ni2-CP		RhNi2-CP		RhNi2-CVD		Rh-CP	
		H_2/CO	T_{max}	H_2/CO	T_{max}	H_2/CO	T_{max}	H_2/CO	T_{max}	H_2/CO	T_{max}	H_2/CO	T_{max}	H_2/CO	T_{max}
500 °C	2/1/20	2.60	583	2.41	591	2.36	590	2.85	579	2.33	600	2.40	595	1.93	595
750 °C	2/1/4	2.00	824	1.98	822	1.92	839	1.85	863	1.95	829	1.94	829	1.94	847
500 °C	2/1/20	2.38	579	2.14	587	2.14	585	2.90	581	2.24	599	2.25	596	2.05	606

Table 5
Gas phase maximum temperature (T_{max}) obtained with mono- and bimetallic catalysts during tests at T_{oven} = 500 °C.

Test		Gas phase temperature/°C	RhNi8-CP	RhNi8-CVD	RhNi2-CP	RhNi2-CVD
CH_4/O_2/He v/v	τ/ms					
2/1/20	65	T_{max}	587	585	599	596
2/1/20	35		630	620	650	645
2/1/40	35		583	583	601	597
2/1/40	17		620	621	649	638

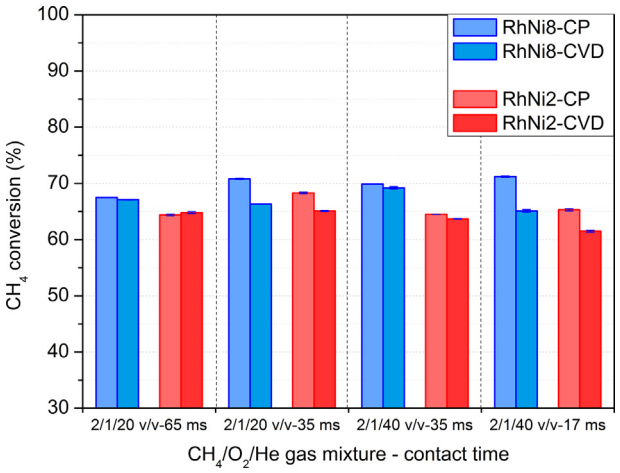

Fig. 8. CH_4 conversion obtained with CP and CVD Rh/Ni bimetallic catalysts during tests at 500 °C by modifying the CH_4/O_2/He gas mixture (2/1/20 and 2/1/4 v/v) and the contact time (65, 35 and 17 ms).

The results above reported seemed to indicate that despite the differences observed in the initial reaction conditions as a function of the preparation method, the catalysts were levelled up after tests at high temperature. As previously reported the reduction of Ni-containing phases could occur with TOS, although also sintering and carbon formation may modify the catalysts features.

To better discern among the stability and activity of CP and CVD catalysts after tests at high temperature, further tests were performed at 500 °C by feeding diluted gas mixtures (2/1/20 and 2/1/40 v/v) and decreasing the contact time value (Fig. 8), and the catalysts were characterized after CPO tests. For both catalyst compositions, CP samples showed higher methane conversion than CVD ones. The differences were more remarkable by feeding the gas mixtures CH_4/O_2/He = 2/1/20 v/v at 35 ms and 2/1/40 v/v at 17 ms; namely, in the catalytic tests in which a higher amount of CH_4 and O_2 were fed to the reactor, and the highest reaction temperatures were recorded (Table 5 and S2). Hence, it appeared that the increase of temperature up to ca. 630–650 °C was not enough to balance the increasing amount of reagent gases to be converted, although the deactivation of the samples cannot be ruled out.

3.3. Characterization of catalysts after CPO tests

PXRD patterns of the samples after catalytic tests (spent catalysts) (Fig. S2) indicated that no large sintering of forsterite, rock-salt and spinel phases occurred in all of the catalysts, despite the severe reaction conditions. Some small differences may be found in the diffraction peak at about $2\theta = 44°$ corresponding to Ni^0. This latter was less intense and broader for RhNi-CP samples in comparison to RhNi-CVD and Ni-CP catalysts, regardless of the Ni content, suggesting differences in metallic particle size (see below TEM results). Some differences were also observed in the specific surface area values of the spent samples, depending on composition and synthesis procedure (Table 1). Only the bimetallic RhNi8-CP catalyst maintained almost the same surface area value than before tests, while the decrease of the surface area was remarkable for catalysts prepared by CVD.

TEM images of spent Ni8-CP catalyst (Fig. 9a) showed a decrease of the mean particle size from 12.1 nm in freshly reduced catalyst to 10.5 nm, with a broad distribution of particle size ranging from 3 to 21 nm (Fig. S3a and b). Conversely, particle size distribution of RhNi8-CVD sample (Fig. 9b) showed a slight increase in comparison to the reduced catalyst centred at 12.5 nm, with a broadening of the distribution (Fig. S3c and d). Lastly, the RhNi8-CP sample (Fig. 9c) showed a more uniform distribution of metal particles, suggesting a marked size redistribution. The fraction of smaller metal particles, that after reduction appeared to be embedded or covered by the oxide support, was not anymore visible, as well as the fraction of largest metal aggregates. The average size of the metal particles decreased to 5.9 nm, i.e. an intermediate value of the size distribution before tests (Fig. S3e and f).

TEM micrographs also highlighted the formation of carbonaceous structured residues such as multiwall carbon nanotubes. Their presence was notably increased in absence of Rh, indeed large nanotubes incorporated into the Ni^0 nanoparticles of Ni8-CP sample, taking them away from the support grains. This occurred to a small extend on RhNi8-CVD samples, while no structured carbon residue grew on the RhNi8-CP sample. Moreover, the average size

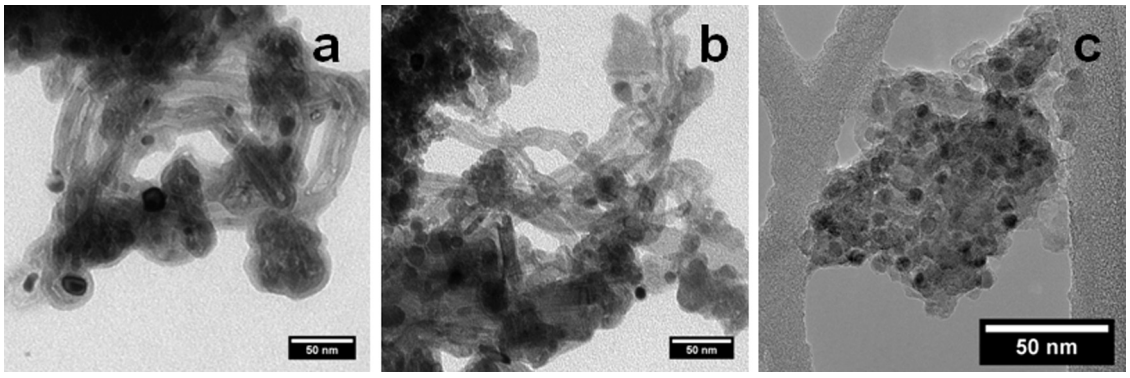

Fig. 9. HRTEM images of Ni8-CP (a), RhNi8-CVD (b) and RhNi8-CP (c) sample after catalytic tests.

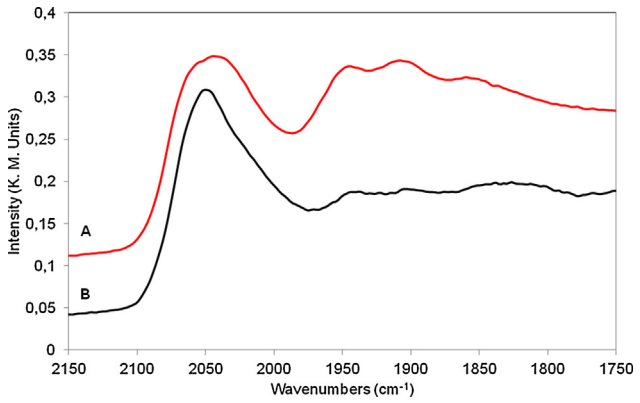

Fig. 10. CO-DRIFT spectra of RhNi8-CVD (trace A, red line) and RhNi2-CVD (trace B, black line) samples after catalytic tests. (For interpretation of the references to colour in this figure legend, the reader is referred to the web version of this article.)

of the metal particles over which the carbon nanotubes had grown was about 10 nm, i.e. the smallest particle contribution to size distribution before the catalytic tests, in agreement with recent studies evidencing that during dry reforming carbon nanotubes grew on the small metal particles [76]. The reduced nanotubes formation on CVD modified samples may be ascribed to the small fraction of pure Ni^0 nanoparticles left on the support by the uneven Rh deposition; whereas these particles were missing in CP samples.

The incorporation of Rh and Ni during the coprecipitation of HT precursors, although may have initially decreased the amount of Rh and Ni species on the catalyst surface after calcination and reduction due to their embedment in the support (such as observed by TEM), gave rise to better performances in terms of catalytic activity and carbon formation. A higher Rh/Ni interaction, starting from the catalyst preparation, the stabilization of the NPs against sintering and carbon formation by the oxide matrix, and the activation of the catalyst with TOS may explain these features. The catalyst activation involved not only the reduction of Ni-containing species, but also the absence of particles embedded in the support. The reduction of Ni during catalytic tests and the high stability of Ni^0 particles in the oxide matrix may explain the differences in the particle size distribution. Namely, small metallic particles were formed during CPO tests due to the reduction with TOS while those obtained during the reduction pretreatment did not sinter.

In CO-DRIFT spectra of RhNi8-CVD and RhNi2-CVD spent samples (Fig. 10) a general reduction of signal intensity without changes in the bands location was observed, which may be related to the coverage of metallic particle surface by carbon, as evidenced by TEM. The amount of CO chemisorbed decreased for both RhNi8-CVD (0.013 $mmol_{CO}/mol_{Ni}$) and RhNi2-CVD (0.008 $mmol_{CO}/mol_{Ni}$) spent catalysts, in agreement with CO-DRIFT data. In the spent RhNi2-CVD catalyst (Fig. 10B) the 2058 cm^{-1} band was still present, evidently convoluted with the 2030 cm^{-1} signal of CO linear on Ni^0 sites, considering its broad shape; lastly, the shoulder at 2075 cm^{-1} disappeared. In the RhNi8-CVD catalyst (Fig. 10A) the same convoluted and broad bands of linear region were still present after reaction tests, while bridged CO signal intensity grew up and the bands at 1949, 1909 and 1864 cm^{-1} may be distinguished.

Both fresh and spent CVD catalysts prepared with the same loading resulted quite similar. In fact, considering bridged/linear CO ratios in DRIFT spectra (Table 3), the reaction tests did not deeply modify the structure; an increase of particle sizes at higher Ni loading was confirmed and also in this case the possible dispersion and reduction effects by Rh addition were quite overturned in 8 wt.% Ni/Rh samples.

4. Conclusions

The coprecipitation of Rh/Ni/Mg/Al HT precursors followed by calcination showed significant advantages for the preparation of bimetallic Rh/Ni catalysts in comparison to the CVD of Rh on reduced Ni HT-derived catalysts, not only because of the high stability of metallic particles in the oxide matrix, but also due to the higher interaction between both elements, which increased the Ni reducibility and dispersion. Consequently, the performances in the catalytic partial oxidation of CH_4 were improved and carbon formation avoided. The Rh/Ni interaction greatly depended on the Rh/Ni atomic ratio, the largest Rh effect was observed on low Ni-loaded catalyst. These data show how enhanced Rh promoting effect may be obtained tuning properly the Rh/Ni atomic ratio.

Acknowledgments

The financial support by the Consiglio Nazionale delle Ricerche (CNR, Roma I) and Ministero dell'Istruzione, Università e Ricerca (MIUR, Roma I) is gratefully acknowledged.

Appendix A. Supplementary data

Supplementary data associated with this article can be found, in the online version, at http://dx.doi.org/10.1016/j.apcatb.2015.05.016

References

[1] V. Dal Santo, A. Gallo, A. Naldoni, M. Guidotti, R. Psaro, Catal. Today 197 (2012) 190–205.
[2] Z. Wei, J. Sun, Y. Li, K. Datye, Y. Wang, Chem. Soc. Rev. 41 (2012) 7994–8008.
[3] T. Inui, K. Saigo, Y. Fujii, K. Fujioka, Catal. Today 26 (1995) 295–302.
[4] B. Li, S. Kado, Y. Mukainakano, T. Miyazawa, T. Miyao, S. Naito, K. Okumura, K. Kunimori, K. Tomishige, J. Catal. 245 (2007) 144–155.
[5] B. Li, S. Kado, Y. Mukainakano, M. Nurunnabi, T. Miyao, S. Naito, K. Kunimori, K. Tomishige, Appl. Catal. A: Gen. 304 (2006) 62–71.
[6] K. Aasberg-Petersen, J.-H. Bak Hansen, T.S. Christensen, I. Dybkjaer, P. Seier Christensen, C. Stub Nielsen, S.E.L. Winter Madsen, J.R. Rostrup-Nielsen, Appl. Catal. A: Gen. 221 (2001) 379–387.
[7] K. Nagaoka, A. Jentys, J.A. Lercher, J. Catal. 229 (2005) 185–196.
[8] A.F. Lucrédio, J.M. Assaf, E.M. Assaf, Biomass Bioenergy 60 (2014) 8–17.
[9] M. García-Diéguez, I.S. Pieta, M.C. Herrera, M.A. Larrubia, L.J. Alemany, Catal. Today 172 (2011) 136–142.
[10] C. Crisafulli, S. Scire, R. Maggiore, S. Minico, S. Galvagno, Catal. Lett. 59 (1999) 21–26.
[11] A. Tanksale, J.N. Beltramini, J.A. Dumesic, G.Q. Lu, J. Catal. 258 (2008) 366–377.
[12] J.A.C. Dias, J.M. Assaf, J. Power Sources 130 (2004) 106–110.
[13] Z. Hou, T. Yashima, Catal. Lett. 89 (2003) 193–197.
[14] N.V. Parizotto, D. Zanchet, K.O. Rocha, C.M.P. Marques, J.M.C. Bueno, Appl. Catal. A: Gen. 366 (2009) 122–129.
[15] K. Takehira, J. Nat. Gas Chem. 18 (2009) 237–259.
[16] C. Fan, Y.-A. Zhu, Y. Xu, Y. Zhou, X.-G. Zhou, D. Chen, J. Chem. Phys. 137 (2012) 014703.
[17] M. Ferrandon, A.J. Kropf, T. Krause, Appl. Catal.: Gen. A 379 (2010) 121–128.
[18] S.L. Lakhapatri, M.A. Abraham, Appl. Catal. A: Gen. 364 (2009) 113–121.
[19] H.-J. Lee, Y.-S. Lim, N.-C. Park, Y.-C. Kim, Chem. Eng. J. 146 (2009) 295–301.
[20] A. Costa Dias, J. Mansur Assaf, J. Power Sources 139 (2005) 176–181.
[21] M. Nurunnabi, Y. Mukainakano, S. Kado, B. Li, K. Kunimori, K. Suzuki, K. Fujimoto, K. Tomishige, Appl. Catal. A: Gen. 299 (2006) 145–156.
[22] Y. Mukainakano, B. Li, S. Kado, T. Miyazawa, K. Okumura, T. Miyao, S. Naito, K. Kunimori, K. Tomishige, Appl. Catal. A: Gen. 318 (2007) 252–264.
[23] J. Kugai, V. Subramani, C. Song, M.H. Engelhard, Y.-H. Chin, J. Catal. 238 (2006) 430–440.
[24] K. Yoshida, K. Okumura, T. Miyao, S. Naito, S. -i. Ito, K. Kunimori, K. Tomishige, Appl. Catal. A-Gen. 351 (2008) 217–225.
[25] J.C.S. Wu, H.-C. Chou, Chem. Eng. J. 148 (2009) 539–545.
[26] B. Koubaissy, A. Pietraszek, A.C. Roger, A. Kiennemann, Catal. Today 157 (2010) 436–439.
[27] A.I. Tsyganok, M. Inaba, T. Tsunoda, K. Uchida, K. Suzuki, K. Takehira, T. Hayakawa, Appl. Catal. A: Gen. 292 (2005) 328–343.
[28] Y.G. Chen, K. Tomishige, K. Yokoyama, K. Fujimoto, Appl. Catal. A: Gen. 165 (1997) 335–347.
[29] B. Pawelec, S. Damyanova, K. Arishtirova, J.L.G. Fierro, L. Petrov, Appl. Catal. A: Gen. 323 (2007) 188–201.
[30] A. Pietraszek, B. Koubaissy, A.-C. Roger, A. Kiennemann, Catal. Today 176 (2011) 267–271.

[31] M. Ocsachoque, F. Pompeo, G. Gonzalez, Catal. Today 172 (2011) 226–231.
[32] A. Le Valant, N. Bion, F. Can, D. Duprez, F. Epron, Appl. Catal. B: Environ. 97 (2010) 72–81.
[33] L.P.R. Profeti, E.A. Ticianelli, E.M. Assaf, Int. J. Hydrogen Energy 34 (2009) 5049–5060.
[34] F. Aupretre, C. Descorme, D. Duprez, D. Casanave, D. Uzio, J. Catal. 233 (2005) 464–477.
[35] U. Izquierdo, V.L. Barrio, J. Requies, J.F. Cambra, M.B. Güemez, P.L. Arias, Int. J. Hydrogen Energy 38 (2013) 7623–7631.
[36] T. Miyata, D. Li, M. Shiraga, T. Shishido, Y. Oumi, T. Sano, K. Takehira, Appl. Catal. A: Gen. 310 (2006) 97–104.
[37] D. Li, I. Atake, T. Shishido, Y. Oumi, T. Sano, K. Takehira, J. Catal. 250 (2007) 299–312.
[38] L. Villegas, N. Guilhaume, C. Mirodatos, Int. J. Hydrogen Energy 39 (2014) 5772–5780.
[39] J. Guo, C. Xie, K. Lee, N. Guo, J.T. Miller, M.J. Janik, C. Song, ACS Catal. 1 (2011) 574–582.
[40] K. Lee, C. Song, M.J. Janik, Langmuir 28 (2012) 5660–5668.
[41] S.L. Lakhapatri, M.A. Abraham, Catal. Sci. Technol. 3 (2013) 2755–2760.
[42] B.C. Enger, R. Lødeng, A. Holmen, Appl. Catal. A 346 (2008) 1–27.
[43] J. Sehested, Catal. Today 111 (2006) 103–110.
[44] F. Basile, G. Fornasari, F. Trifirò, A. Vaccari, Catal. Today 64 (2001) 21–30.
[45] F. Basile, G. Fornasari, F. Trifirò, A. Vaccari, Catal. Today 77 (2002) 215–223.
[46] D.V. Cesar, M.A.S. Baldanza, C.A. Henriques, F. Pompeo, G. Santori, J. Múnera, E. Lombardo, M. Schmal, L. Cornaglia, N. Nichio, Int. J. Hydrogen Energy 38 (2013) 5616–5626.
[47] Y. Ji, W. Li, H. Xu, Y. Chen, Catal. Lett. 71 (2001) 45–48.
[48] B.C. Enger, R. Lødeng, A. Holmen, Catal. Lett. 134 (2010) 13–23.
[49] B.C. Enger, R. Lødeng, A. Holmen, Appl. Catal. A: Gen. 364 (2009) 15–26.
[50] C. Berger-Karin, J. Radnik, E.V. Kondratenko, J. Catal. 280 (2011) 116–124.
[51] A. Horváth, G. Stefler, O. Geszti, A. Kienneman, A. Pietraszek, L. Guczi, Catal. Today 169 (2011) 102–111.
[52] J.J. Strohm, J. Zeng, C. Song, J. Catal. 238 (2006) 309–320.
[53] A.F. Lucrédio, J.M. Assaf, E.M. Assaf, Appl. Catal. A: Gen. 400 (2011) 156–165.
[54] H. Tanaka, R. Kaino, K. Okumura, T. Kizuka, Y. Nakagawa, K. Tomishige, Appl. Catal. A: Gen. 378 (2010) 175–186.
[55] M. Gazzano, W. Kagunya, D. Matteuzzi, A. Vaccari, J. Phys. Chem. 101 (1997) 4514–4519.
[56] D.H. Kim, J.S. Kang, Y.J. Lee, N.K. Park, Y.C. Kim, S.I. Hong, D.J. Moon, Catal. Today 136 (2008) 228–234.
[57] J.C. Vargas, E. Vanhaecke, A.C. Roger, A. Kiennemann, Stud. Surf. Sci. Catal. 147 (2004) 115–120.
[58] F. Romero-Sarria, J.C. Vargas, A.C. Roger, A. Kiennemann, Catal. Today 133–135 (2008) 149–153.
[59] J.H. Jeong, J.W. Lee, D.J. Seo, Y. Seo, W.L. Yoon, D.K. Lee, D.H. Kim, Appl. Catal. A: Gen. 302 (2006) 151–156.
[60] K. Nakagawa, N. Ikenaga, Y. Teng, T. Kobayashi, T. Suzuki, Appl. Catal. A: Gen. 180 (1999) 183–193.
[61] V.R. Choudhary, B. Prabhakar, A.M. Rajput, J. Catal. 157 (1995) 752–754.
[62] S. Albertazzi, F. Basile, P. Benito, P. Del Gallo, G. Fornasari, D. Gary, V. Rosetti, A. Vaccari, Catal. Today 128 (2007) 258–263.
[63] F. Basile, P. Benito, G. Fornasari, D. Gazzoli, I. Pettiti, V. Rosetti, A. Vaccari, Catal. Today 142 (2009) 78–84.
[64] V. Dal Santo, C. Mondelli, V. De Grandi, A. Gallo, S. Recchia, L. Sordelli, R. Psaro, Appl. Catal. A: Gen. 346 (2008) 126–133.
[65] V. Dal Santo, A. Gallo, M.M. Gatti, V. De Grandi, R. Psaro, L. Sordelli, S. Recchia, J. Mater. Chem. 19 (2009) 9030–9037.
[66] A. Beretta, A. Donazzi, G. Groppi, P. Forzatti, V. Dal Santo, L. Sordelli, V. De Grandi, R. Psaro, Appl. Catal. B: Environ. 83 (2008) 96–109.
[67] R. Ugo, C. Dossi, R. Psaro, J. Mol. Catal. A: Chem. 107 (1996) 13–22.
[68] A. Gallo, C. Pirovano, M. Marelli, R. Psaro, V. Dal Santo, Chem, Vap. Deposition 16 (2010) 305–310.
[69] W.K. Jozwiak, M. Nowosielska, J. Rynkowski, Appl. Catal. A: Gen. 280 (2005) 233–244.
[70] V. Dal Santo, C. Dossi, A. Fusi, R. Psaro, C. Mondelli, S. Recchia, Talanta 66 (3) (2005) 674–682.
[71] C. Mondelli, V. Dal Santo, A. Trovarelli, M. Boaro, A. Fusi, R. Psaro, S. Recchia, Catal. Today 113 (2006) 81–86.
[72] G. Poncelet, M.A. Centeno, R. Molina, Appl. Catal. A: Gen. 288 (2005) 232–242.
[73] M. Primet, J.A. Dalmon, G.A. Martin, J. Catal. 46 (1977) 25–36.
[74] J.B. Peri, J. Catal. 86 (1984) 84–94.
[75] J. Hofer, J. Solid State Chem. 45 (1982) 303–308.
[76] K. Mette, S. Kühl, H. Düdder, K. Kähler, A. Tarasov, M. Muhler, M. Behrens, ChemCatChem 6 (2014) 100–104.